Editors' Suggestion

Low-temperature anomalies of a vapor deposited glass

Beatriz Seoane,[1,2] Daniel R. Reid,[3] Juan J. de Pablo,[3] and Francesco Zamponi[1]

[1]*Laboratoire de physique théorique, Département de physique de l'ENS, École normale supérieure, PSL Research University, Sorbonne Université, CNRS, 75005 Paris, France*

[2]*Instituto de Biocomputación y Física de Sistemas Complejos (BIFI), 50009 Zaragoza, Spain*

[3]*Institute for Molecular Engineering, University of Chicago, 5640 South Ellis Avenue, Chicago, Illinois 60637, USA*

(Received 5 October 2017; revised manuscript received 24 November 2017; published 29 January 2018)

We investigate the low-temperature properties of two-dimensional Lennard-Jones glass films, prepared *in silico* both by liquid cooling and by physical vapor deposition. We identify deep in the solid phase a crossover temperature T^*, at which slow dynamics and enhanced heterogeneity emerge. Around T^*, localized defects become visible, leading to vibrational anomalies as compared to standard solids. We find that, on average, T^* decreases in samples with lower inherent structure energy, suggesting that such anomalies will be suppressed in ultrastable glass films, prepared both by very slow liquid cooling and vapor deposition.

DOI: 10.1103/PhysRevMaterials.2.015602

Low-temperature crystalline solids are usually described in terms of harmonic vibrations around a perfect periodic lattice (phonons). Within this framework, defects such as vacancies and dislocations can be treated as small perturbations. This description breaks down for amorphous solids such as glasses, foams, emulsions, plastics, colloids, granular materials, bacterial colonies, and tissues [1–7]. In these systems, the identification of "defects" becomes challenging because the solid ground state is strongly disordered. As a consequence, amorphous solids display many universal *anomalies* with respect to crystals. Examples are the so-called boson peak, an excess of low-energy vibrational modes [8]; the anomalous scaling of heat capacity and thermal conductivity with temperature [9,10]; the irreversible plastic response to arbitrarily small perturbations [1,3,4,11]; and highly cooperative relaxation dynamics, contributing to the so-called β processes [12–14].

These anomalies have been widely reported in amorphous solids of very different nature. Interestingly, recent experimental work has shown that by preparing glasses through a process of physical vapor deposition, one can produce ultrastable states that lie deep in the free-energy landscape [15]. Compared to their liquid cooled counterparts, vapor deposited glasses show higher density [16] and kinetic stability [15,17]. When these ultrastable glasses are studied at very low temperatures, it is found that the anomalies characteristic of amorphous solids are strongly suppressed [18–22].

Many theoretical approaches to this problem are based on the study of the potential energy landscape of glass-forming particle systems [13,23–28]. These studies have suggested that glass anomalies can be interpreted in terms of glass states being not well-defined energy minima, but structured metabasins containing a collection of subbasins separated by barriers of variable size [29,30] (see Fig. 1). In particular, recent work [31–33] has identified a set of simple observables (the mean square displacement between identical "clones" of the original system) that allows one to detect easily the development of a structure of subbasins inside a glass metabasin.

In this work, using the methods of [31–33], we explore *in silico* the potential energy landscape of binary Lennard-Jones glass films prepared through two experimentally relevant protocols: slow liquid cooling and physical vapor deposition following Ref. [34]. We study these films due to their experimental relevance and the fact that they have been well characterized by previous work [34,35]. In contrast to previous studies which prepared bulk equilibrium samples using the swap algorithm [32,33], our film preparation methods, inspired by the vapor deposition experimental protocol, produce nonequilibrium films that are expected to be higher in the potential energy landscape than experimentally prepared vapor deposited glasses [36,37]. In addition, both our liquid cooled and vapor deposited films are prepared in the presence of both a substrate and a free surface, allowing the study of these features' influence on the low-temperature physics of the samples.

We find that a threshold T^* can be detected within the glass phase, below which vibrational dynamics of the solid becomes orders of magnitude slower and the structure of the glass basin becomes visible. The value of T^* depends primarily on film stability, decreasing substantially with the inherent structure energy of the sample, a measure of stability [35], while a protocol dependence of T^* is not detected. This observation is compatible with the disappearance of anomalies in ultrastable glasses. Furthermore, we observe significant sample-to-sample variations both in the value of T^* and in the aging dynamics below this threshold. All samples display localized defects, however, several samples display collective dynamics, which could be related to cooperative displacements enabled by the free surface. It is important to note that the glasses considered here incorporate the nonequilibrium nature of real materials, as well as the presence of a substrate and free boundary, which have an important impact on the physics below T^*. Note also that the films considered in this study have fixed thickness (the same used in Ref. [34]), so the dependence of the results on films' thickness is not addressed here and left for future work.

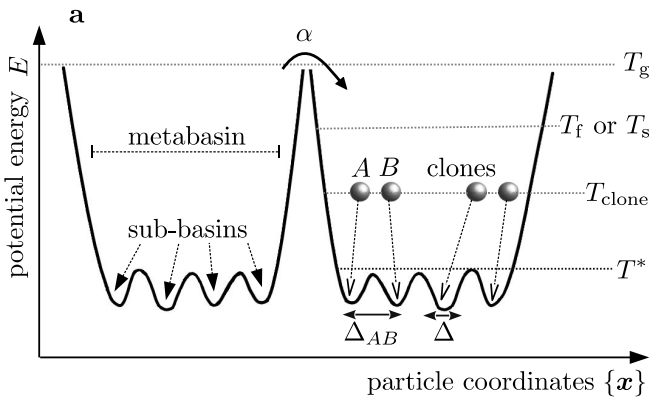

FIG. 1. Illustration of the energy landscape. Samples are prepared in a glass basin at temperature T_f or T_s lower than the glass transition T_g. They are then brought at lower temperature T_{clone} to ensure that no residual diffusion (α relaxation) is present. There, clones are produced to sample the interior of glass basins. Our main observables are $\Delta(t,t_w)$, the mean square displacement of particles in a single clone, and $\Delta_{AB}(t_w)$, the displacement between two distinct clones.

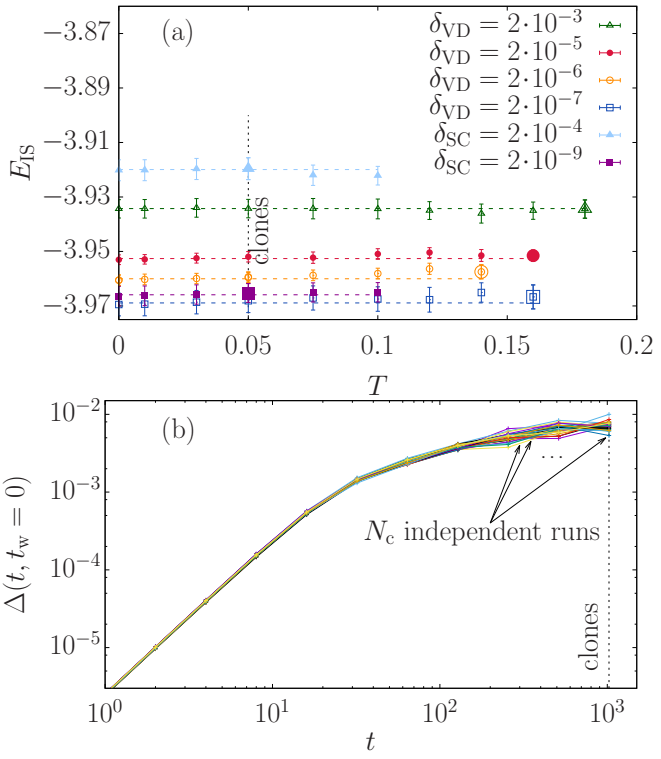

FIG. 2. Preparation of glass samples and clones. (a) Inherent structure energy E_{IS} measured at T_f or T_s (larger symbol), and upon cooling or heating the samples at different T. Dashed lines are constant fits to the data for $T \leqslant T_{clone} = 0.05$, that demonstrate that the system is not leaving its metabasin. (b) $\Delta(t,t_w = 0)$ at temperature $T = T_{clone}$ for one of the VD samples prepared with $\delta_{VD} = 2 \times 10^{-6}$. The length of the clone preparation simulations is indicated by the dotted line, whose length is the size of the cage (i.e., the height of the plateau).

I. SAMPLE PREPARATION PROTOCOL

Here, we provide a brief description of the system and protocols used in this work. See Ref. [34], the illustration in Fig. 1, and the Appendices for details. We prepare N_s glass *samples* of a binary two-dimensional Lennard-Jones system which shows a glass transition temperature close to $T_g \approx 0.21$ for the range of cooling rates used in this study. We study two distinct classes of films: (i) those formed by slow cooling (SC) of liquid films into the glass phase at a final temperature T_f with two distinct cooling rates δ_{SC}, and (ii) those formed by a procedure mimicking physical vapor deposition (VD). In VD, we use four different deposition rates δ_{VD} with substrates held at temperature T_s. In both protocols, $T_f < T_g$ or $T_s < T_g$, so the samples we produce are in the glass phase.

To study the vibrational anomalies of a glass basin, each sample is brought to a lower temperature T_{clone} (lower than either T_f or T_s). The same T_{clone} is employed in all cases, i.e., for all samples and all protocols. At this temperature, the system is sufficiently close to its inherent structure. In fact, as shown in Fig. 2(a), the inherent structure energy (as computed by energy minimization configurations at different temperatures) remains constant below this temperature for all the glasses considered. From this, we suggest that no diffusion occurs over this period. We verify that the system behaves as a normal solid at T_{clone}, meaning that the state is ergodic and the vibrations of the particles are weakly correlated. Once cooled, we prepare N_c *clones*, or independent configurations distributed within the basin of each glass sample. In practice, each clone is obtained as the result of an independent simulation of length t_{clones}, the dotted line in Fig. 2. The clones are then instantaneously quenched to a final temperature $T < T_{clone}$ and their dynamics is examined at constant T, with t_w being the time elapsed since the quench. Note that when samples are studied at $T = T_{clone}$, the dynamics is stationary, and for this reason the origin of time can be chosen arbitrarily.

Following previous work [31–33], we focus our attention on two observables:

$$\Delta(t + t_w, t_w) = \frac{1}{N}\sum_{i=1}^{N} \overline{\langle |\boldsymbol{r}_i(t + t_w) - \boldsymbol{r}_i(t_w)|^2 \rangle}\,, \qquad (1)$$

which is the mean square displacement of particles in each clone between time t_w and $t + t_w$, and

$$\Delta_{AB}(t_w) = \frac{1}{N}\sum_{i=1}^{N} \overline{\langle |\boldsymbol{r}_i^A(t_w) - \boldsymbol{r}_i^B(t_w)|^2 \rangle}, \qquad (2)$$

which is the mean square displacement between particles in two distinct clones (denoted A and B) of the same sample at the same time t_w, $\{\boldsymbol{r}_i^A(t_w)\}$ and $\{\boldsymbol{r}_i^B(t_w)\}$. Here, $\langle \dots \rangle$ refers to the thermal average, computed as the average over all the clones of the same sample, while $\overline{\cdots}$ refers to the average over all the samples with the same preparation procedure. To increase the statistics, the thermal average of Δ_{AB} is computed using all the $N_c(N_c - 1)/2$ possible couples of A and B clones, but the error bars are computed by taking into account the correlations between pairs using the jackknife method [38].

Both quantities are computed for particles in the middle region of the sample (the region in-between the two horizontal lines in Fig. 8). In this region, the density and relative

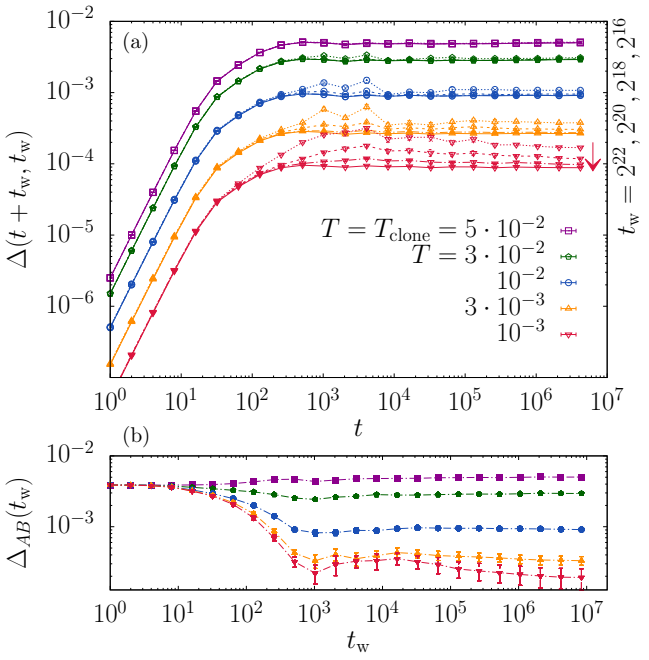

FIG. 3. Emergence of slow vibration dynamics. (a) Aging effects in $\Delta(t+t_w,t_w)$ for VD glasses obtained with $\delta_{VD} = 2\times\ 10^{-6}$. For each temperature, we plot four values of t_w (2^{16},2^{18},2^{20},2^{22}), all of them corresponding to the regime where the ballistic part has converged to the same curve. (b) Aging effects in $\Delta_{AB}(t_w)$.

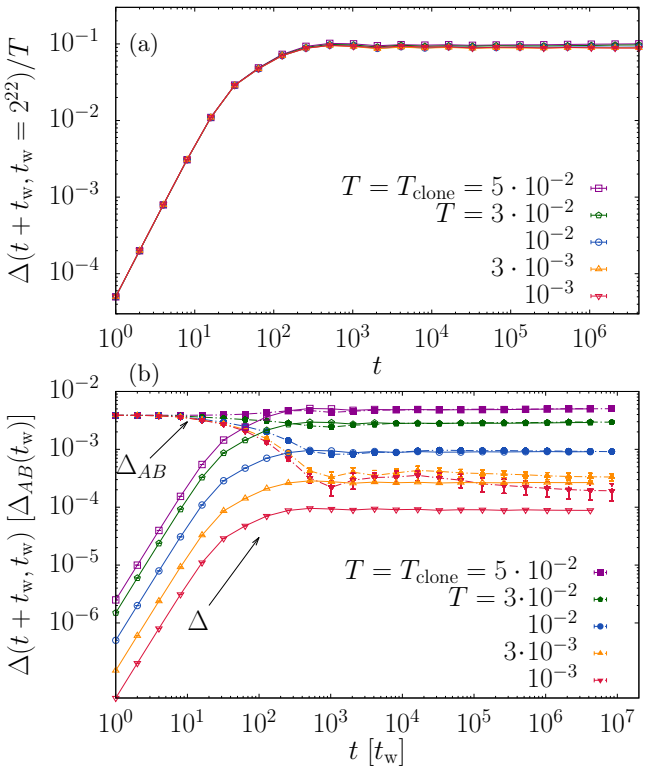

FIG. 4. Breakdown of the ergodicity. (a) The scaled $\Delta(t+t_w,t_w)/T$ for the largest $t_w = 2^{22}$, at different temperatures. There is an excellent collapse indicating that for large t_w the MSD is proportional to temperature. (b) We compare $\Delta(t+t_w,t_w)$ for $t_w = 2^{22}$ vs t with $\Delta_{AB}(t_w)$ vs t_w of Fig. 3. The onset where $\Delta^{\infty}_{AB} = \Delta_{AB}(t_w\to\infty) \neq \Delta(t\to\infty,t_w\to\infty) = \Delta^{\infty}$ corresponds to the emergence of aging of Fig. 3(a).

concentration of the two particle types are both constant [34], allowing boundary effects to be avoided. The displacement of the center of mass of the whole sample is removed. Both observables are averaged over clones and, unless otherwise specified, over multiple samples prepared with the same protocol.

II. RESULTS

A. Clones are prepared in an ergodic state

We begin by discussing the behavior of $\Delta(t+t_w,t_w)$ and $\Delta_{AB}(t_w)$ for samples at the clone preparation temperature T_{clone} (see purple squares in Fig. 3). Because clones have been prepared well below T_g, no diffusion is observed in our simulation time windows, meaning that the averaged cage size Δ^{∞} of the material at each temperature can be extracted from the plateau value of $\Delta(t+t_w,t_w)$ at long t_w, as shown in Fig. 3(a). On the other hand, $\Delta_{AB}(t_w)$ reach a constant value at long times [see Fig. 3(b)] that precisely coincides with Δ^{∞} [it can be better appreciated in Fig. 4(b) where both observables are plotted superimposed]. The convergence of these two quantities in the long time limit means that a single trajectory of the system samples, at long times, the same states that are sampled by two independently prepared clones. This indicates that the glass basin is comprised of well-defined internal cages which are ergodically sampled, and that vibrations of particles remain weakly correlated [32,33,39].

B. Growing time scales upon cooling

Next, we study the behavior of $\Delta(t+t_w,t_w)$ and $\Delta_{AB}(t_w)$ as a function of t, using different reference times t_w elapsed after a sudden drop in temperature from T_{clone} to $T < T_{clone}$ (Fig. 3). At small values of t_w, one expects a sharp nonequilibrium response of $\Delta(t+t_w,t_w)$ and $\Delta_{AB}(t_w)$ to the change of temperature: this is manifested both at small t, during the ballistic exploration of the cages, and at long t in the plateau region. The value of the plateau evolves from the typical cage size at the preparation temperature (at very small t_w) to the new temperature one (longest t_w) (see Fig. 3). In addition, as we show in Fig. 4(a), the limiting long-t_w curves at different temperatures can be roughly collapsed in a single curve by dividing them by the temperature, which suggests that the size of the cages increases linearly with temperature. However, the typical time it takes to the system to converge to this long-t_w plateau depends drastically on the final temperature. This is more clearly seen by plotting $\Delta(t+t_w,t_w)/T$ for $t = 2^{22}$ [i.e., the long-t limit of the mean square displacement (MSD)] as function of t_w [see Fig. 5(a)]. While at high temperatures the plateau converges rapidly to its final value, this convergence slows significantly as the temperature is decreased. In order to quantify this effect, we extract the time τ such that for $t_w > \tau$, the value of $\Delta(2^{22}+t_w,t_w)/T$ is consistently below a threshold [dashed line in Fig. 5(a)]. We fixed the threshold to 0.2 for all the samples. The errors are obtained using the jackknife method [38]. We show τ as a function of T, for glasses prepared by different protocols in Fig. 5(b), finding

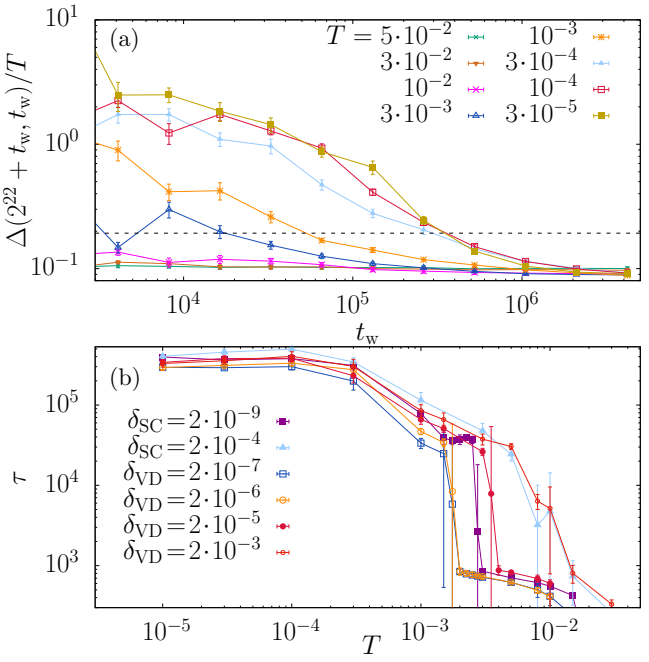

FIG. 5. Convergence to the plateau. (a) The plateau height [long-t limit of $\Delta(t+t_w,t_w)/T$, estimated by the largest available t] as function of t_w for different temperatures, extracted from the data of Fig. 4(a). (b) The time τ needed to fall below the dashed line in (a), as a function of T for differently prepared glasses.

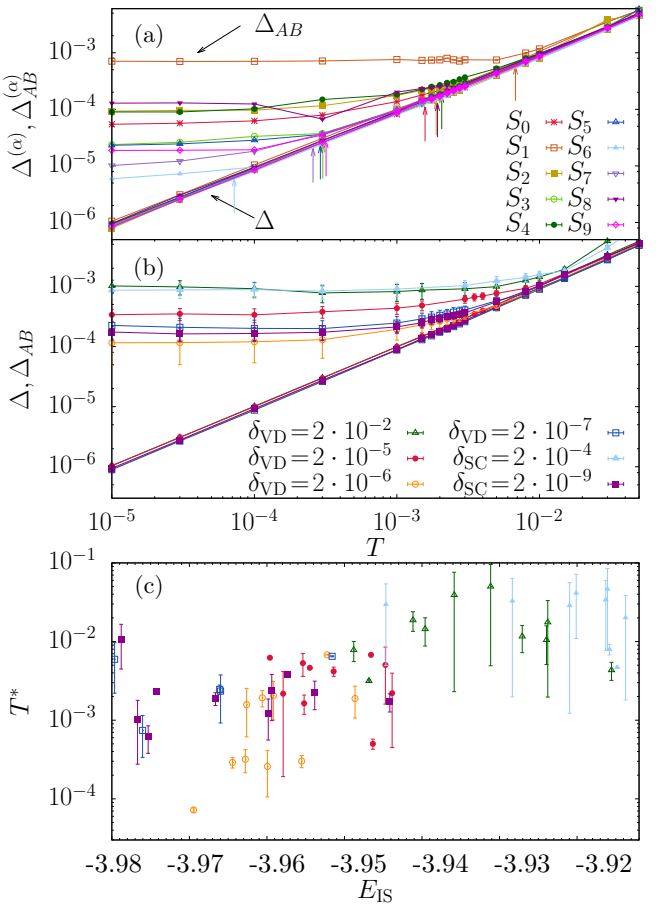

FIG. 6. Exponential decay of T^* with the inherent structure energy of the samples. (a) Individual long time values of Δ^∞ and Δ^∞_{AB}, plotted versus T, for the 10 VD glass samples obtained with $\delta_{VD} = 2 \times 10^{-6}$. The separation of Δ^∞ and Δ^∞_{AB} happens at a strongly sample-dependent temperature. (b) Averages of Δ^∞ and Δ^∞_{AB} over samples, plotted versus T, for different sample preparation protocols, showing that the average separation temperature depends on the preparation protocol and decreases for slower protocols. (c) Values of T^* as function of the inherent structure energy, as extracted sample by sample for the different preparation protocols [different colors with the same color code as in (b)], showing a high correlation between E_{IS} and T^*.

that these characteristic times grow very quickly in the vicinity of well-defined temperatures that depend on how the material was prepared. Of course, within this approach, the values of τ depend of the threshold chosen, and we observed that the temperatures at which the sharp growth occurs also shift mildly (effect included in the error bars). Nevertheless, the overall picture remains the same.

Furthermore, the convergence to the final cage sizes [Fig. 3(a)] slows at roughly the same temperatures at which $\Delta(t+t_w,t_w)$ and $\Delta_{AB}(t_w)$ no longer converge to the same plateau value at long times, as shown in Fig. 4(b). The large time limit of both quantities, which we call Δ^∞ and Δ^∞_{AB}, plotted as a function of T [Fig. 6(b)], converge to the same values at high temperatures ($T \gtrsim 10^{-2}$), while they clearly separate at low temperatures. It is, however, important to note that the relaxation time τ [Fig. 5(b)] does not seem to diverge at any finite temperature: instead, it saturates. One may wonder whether this saturation is simply due to the finite size of the system, in which case the value of τ at low temperature would increase with system size. Ruling out this possibility would require a careful finite-size study, that we leave for future work.

C. Temperature threshold and inherent structure energy

We have seen that the long time limits Δ^∞ and Δ^∞_{AB} separate near a threshold T^*, indicating a loss of ergodicity within the glass basin below this temperature, which is also associated with the emergence of much slower aging dynamics. If we examine each sample individually, we find that the value of T^* fluctuates strongly from sample to sample [Fig. 6(a)], and it depends strongly on how the sample was prepared, as we show in Fig. 6(b) by taking the sample averages.

To study systematically the dependence of T^* on sample preparation method and rate, we define it more precisely as follows. We compute the temperature below which Δ^∞ and Δ^∞_{AB} become distinct in each sample, and the temperature for which $\Delta^\infty(T) = \Delta^\infty_{AB}(T = 10^{-5})$, i.e., the point at which a horizontal line equal to the zero-temperature value of Δ^∞_{AB} intersects $\Delta^\infty(T)$. We define T^* as the average of these two estimations [indicated by the arrows in Fig. 6(a)], and we associate to it an error given by half the difference of these two estimations. The reason for this is that T^* does not correspond to a sharp phase transition but rather to a crossover, therefore, one cannot define T^* unambiguously. We show the results for the T^* of each sample in Fig. 6(c) as function of their inherent structure energy, which is correlated with the cooling or depo-

sition rate and is a proxy for glass stability [34,35]. In spite of the large spread of the data points, we find that the values of the logarithms of the T^* are correlated (the linear correlation coefficient is 0.67) with the inherent structure energies of the samples, suggesting that the threshold temperature T^* decreases with the inherent structure energy (roughly exponentially). Based on this finding, we suggest that experimental ultrastable glasses, that typically lie in energy minima below the ones accessible in our numerical simulations, would see the anomalies discussed in this work strongly suppressed, as in that case T^* would be extremely low or even absent.

D. Aging and heterogeneity of individual samples

We now investigate in greater detail the behavior of individual samples in the regime of times and temperatures where aging dynamics is slow. To this end, in addition to the mean square displacements defined above, we introduce the displacement of individual particles in two clones, $u_i(t_w) \propto |\boldsymbol{r}_i^A(t_w) - \boldsymbol{r}_i^B(t_w)|^2$, normalized in such a way that $(1/N)\sum_i \langle u_i(t_w)\rangle = 1$, and following Ref. [33] we introduce a susceptibility

$$\chi_{AB}(t_w) = \frac{\sum_{ij}[\langle u_i(t_w)u_j(t_w)\rangle - \langle u_i(t_w)\rangle\langle u_j(t_w)\rangle]}{\sum_i[\langle u_i(t_w)^2\rangle - \langle u_i(t_w)\rangle^2]}, \quad (3)$$

that is equal to 1 if $u_i(t_w)$ and $u_j(t_w)$ are uncorrelated for all $i \neq j$, while otherwise it gives an estimate of the correlation length of particle displacements (raised to an unknown power). It has been suggested by previous work [28,31,32] that, below the threshold T^*, the system might be "marginally stable," i.e., characterized by a diverging correlation length of particle displacements, and a diverging χ_{AB}, also associated to delocalized soft vibrational modes [40,41]. However, Ref. [33] found, in a system similar to ours, that χ_{AB} always remains small, suggesting that the low-temperature phase is not marginally stable.

In Fig. 7 we report the aging behavior of $\Delta_{AB}(t_w)$ and $\chi_{AB}(t_w)$ for two individual representative samples, labeled as samples 1 and 9. In sample 1, we do not observe aging in either $\Delta_{AB}(t_w)$ or $\chi_{AB}(t_w)$, which are independent of t_w. The susceptibility displays only a moderate increase upon decreasing temperature below $T^{*(1)}$, which is consistent with the results of Ref. [33]. In sample 9, instead, we observe strong aging in $\Delta_{AB}(t_w)$ around $T^{*(9)}$, and correspondingly the susceptibility increases by a factor of about 20 at intermediate times and $T \sim T^{*(9)}$, before relaxing to smaller values at longer times.

To provide a real space interpretation of these findings, in Fig. 8 we display snapshots of the displacement field $\langle u_i(t_w)\rangle$, averaged over clones, for the same two representative samples, at several values of T and t_w. Both samples display, during the aging, a collective displacement of the upper part of the sample, corresponding to a global increase of density upon cooling (an effect related to the existence of a free surface), as well as clearly visible localized defects. The main difference between the two samples is that in sample 9 the surface process leads to greater displacement between clones, indicating that this process happens in a more heterogeneous way from clone to clone, leading to the stronger aging visible in both Δ_{AB} and χ_{AB}. The localized defects are compatible with those observed in Ref. [33] and lead to a separation of Δ^∞ and Δ^∞_{AB} at low

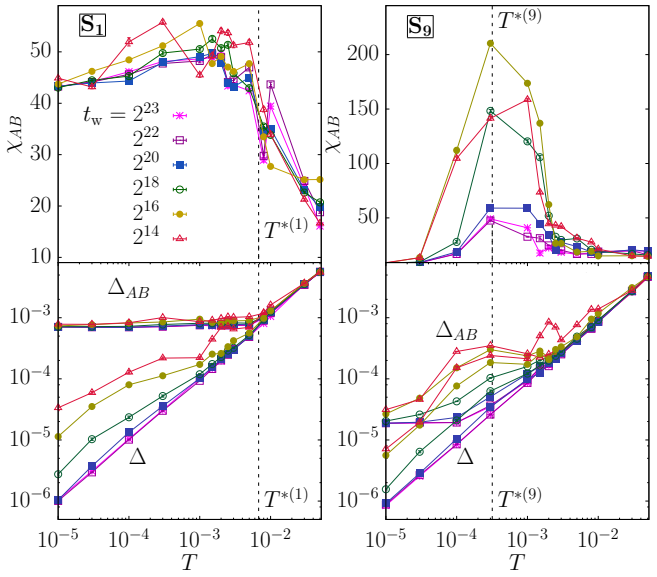

FIG. 7. Aging behavior of two representative samples. Values of $\chi_{AB}(t_w)$ (top) and of $\Delta_{AB}(t_w)$, $\Delta(2^{22}+t_w,t_w)$ (bottom) for two representative VD samples obtained with $\delta_{VD} = 2 \times 10^{-6}$, plotted as a function of temperature T for several values of t_w. The two samples (labeled 1 and 9) have $e_{IS}^{(1)} = -3.9522$ and $e_{IS}^{(9)} = -3.9628$. Sample 1 displays no aging aside from the one related to the convergence of $\Delta(2^{22}+t_w,t_w)$ to its long time limit at low T and only a moderate increase of χ_{AB} upon lowering temperature. Sample 9 displays strong aging around its $T^{*(9)}$, accompanied by a large growth of χ_{AB}.

temperatures that is not accompanied by aging nor by a large χ_{AB}. We thus conclude that the system is not marginally stable below T^*.

III. DISCUSSION

We have identified, independently for each sample (or glass basin), a threshold temperature T^*, located deep in the glass phase. Around this temperature, the aging dynamics after a quench becomes slow, and vibrational heterogeneity is enhanced. Below T^*, aging dynamics remains slow, and localized defects appear, similar to the ones reported in Refs. [33,42]. The threshold, however, does not correspond to a sharp phase transition and excitations are localized below T^*.

Our main result is that T^* markedly decreases with decreasing E_{IS} and thus increasing film stability [34,35]. Hence, ultrastable glasses with low E_{IS} are also predicted to display a very low T^* and thus remain normal solids down to extremely low temperatures. Our results qualitatively agree with previous studies [32,33], but they are obtained for nonequilibrium films, formed through realistically simulated liquid cooling and physical vapor deposition processes, that sit higher in the energy landscape [37].

The theoretical interpretation of our findings is challenging. Localized defects of different nature have been discussed in the context of glasses (see, e.g., [1–7,43–46]), and our findings could be related to at least some of those theoretical proposals. Future work should clarify these connections, both by additional numerical simulations and analytical calculations. The emergence of slow dynamics at low temperature, accompanied

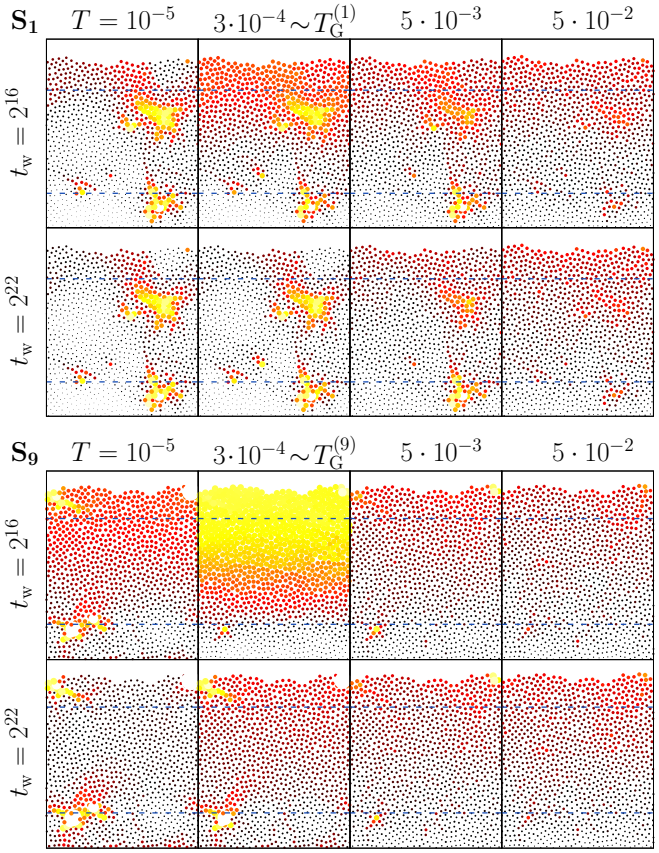

FIG. 8. Snapshots of the displacement field. The displacement field $\langle u_i(t_w)\rangle$, averaged over clones, is shown for the same two representative samples as in Fig. 7. For each particle i, the corresponding displacement is shown as a circle centered in the particle position, whose area is proportional to $\langle u_i(t_w)\rangle$. The colors help visualizing the largest displacements. Sample 1 displays only localized defects, while sample 9 displays, at intermediate times and $T \sim T^{*(9)}$, a collective displacement of the upper part of the sample.

by the nontrivial change in the vibrations of the particles, is reminiscent of the mean field scenario where these features are consequences of an underlying phase transition, called the Gardner transition [47,48], which separates a high-temperature normal solid and a low-temperature marginally stable solid. While our results, similarly to those of Refs. [33,42], suggest that no sharp phase transition takes place in our samples, one could speculate that the localized excitations we identified are some kind of "vestige" of an avoided Gardner-type transition. Because numerical simulations of hard sphere (colloidal) glasses are instead consistent with the existence of a transition [32], it becomes very important to understand which systems display such a transition and which do not, and why. This is a very important direction for future work, analytical [49–53], numerical [31–33,42,54], and experimental [39,55].

In conclusion, our observations may explain why some anomalies characteristic of amorphous solids are suppressed in ultrastable glasses, but more work is needed to relate precisely the anomalies observed in our numerically simulated samples to the ones observed in experiments [18–22]. Moreover, finite-size effects, and in particular the dependence of our results on films' thickness, remain to be investigated.

ACKNOWLEDGMENTS

We thank G. Biroli, L. Berthier, M. Ediger, G. Parisi, C. Scalliet, and P. Urbani for useful exchanges about this work, and J. Helfferich for his help at the early step of this work. This work was granted access to the HPC resources of MesoPSL financed by the Region Ile de France and the project Equip@Meso (Reference No. ANR-10-EQPX-29-01) of the programme Investissements d'Avenir supervised by the Agence Nationale pour la Recherche. Fast GPU-accelerated codes for simulation of glassy materials were developed with support from DOE, Basic Energy Sciences, Materials Research Division, under MICCoM (Midwest Integrated Center for Computational Materials). This project has received funding from the European Union's Horizon 2020 research and innovation program under the Marie Skłodowska-Curie Grant Agreement No. 654971. This work was partially supported through Grant No. FIS2015-65078-C2-1-P, jointly funded by Ministerio de Economía, Industria y Competitividad (Spain) and European Regional Development Fund. This work was financially supported by a grant from the Simons Foundation (Grant No. 454955, F.Z.), and by a DMREF Grant No. NSF-DMR-1234320.

APPENDIX A: DETAILS OF THE SYSTEM

We work with films of a binary mixture of $N = 1200$, two-dimensional Lennard-Jones particles of types 1 and 2 (where 1 is more common with concentration $\chi_1 \equiv N_1/N \sim 65\%$) that interact with a third type of particle 3 that act as a fixed substrate at the bottom of the simulation box. The upper boundary in the vertical axis remains open and we consider periodic boundary conditions in the direction parallel to the substrate. The interaction potential between particles of two species α,β separated by a distance r is

$$u_{\alpha,\beta}(r) = 4\epsilon_{\alpha,\beta}\left[\left(\frac{\sigma_{\alpha,\beta}}{r}\right)^{12} - \left(\frac{\sigma_{\alpha,\beta}}{r}\right)^{6}\right] \qquad \text{(A1)}$$

for $r < r_{\text{cutoff}}^{\alpha,\beta}$, and zero otherwise. The cutoff distances are $r_{\text{cutoff}}^{\alpha,\beta} = 2.5\sigma_{\alpha,\beta}$, being the particle diameters $\sigma_{11} = 1.0\sigma$, $\sigma_{22} = 0.88\sigma$, $\sigma_{33} = 0.6\sigma$, $\sigma_{12} = 0.8\sigma$, $\sigma_{13} = 0.75\sigma$, $\sigma_{23} = 0.75\sigma$. For the potential we use the values $\epsilon_{11} = 1.0\epsilon$, $\epsilon_{22} = 0.5\epsilon, \epsilon_{33} = 0.1\epsilon, \epsilon_{12} = 1.5\epsilon, \epsilon_{13} = 1.0\epsilon, \epsilon_{23} = 1.0\epsilon$. All quantities in the paper are shown in Lennard-Jones units, that is, σ, ϵ, and mass m are equal to 1, and time is thus in units of $\sigma\sqrt{m/\epsilon}$. Energies in the paper were measured without shifting the potential to zero at the cutoff distance, a choice that has no impact during the simulation considering that updates in the molecular dynamics algorithm only depend on the derivatives of the interaction potential $u_{\alpha,\beta}(r)$. The discrepancies between the inherent structure energies of this work and the ones shown in Ref. [34] come from the fact that in the previous work, energies were rescaled to compare configurations with exactly the same portion of type-1 particles in the bulk. The temperature is fixed using a Nosé-Hoover thermostat [56] with a temperature damping parameter $100\Delta t$, where the time step is here $\Delta t = 0.005$. Inherent structural energies were calculated by minimizing configurations using the FIRE algorithm with energy and force tolerances of 10^{-10} [57]. All simulations were performed using LAMMPS [58].

Because ϵ_{12} is higher than ϵ_{11} and ϵ_{22}, the most stable configurations tend to maximize the $1-2$ interactions, which, considering that type 1 particles are more abundant, tends to displace the particles of type 1 towards the surface, creating a clear nonhomogeneity along the axis perpendicular to the substrate. In order to avoid the effect of these two boundaries, all the quantities computed in this paper were measured using only the particles in bulk, which corresponds to the central 60% region (see, for example, the region in-between the two horizontal lines in Fig. 8 of the main text). The number of particles in the bulk varies from sample to sample, but it remains equal to $N_{\text{bulk}} \sim 660$–670.

APPENDIX B: PREPARATION OF GLASS SAMPLES

We prepare glass configurations following two distinct protocols: slow cooling from the liquid phase (SC) with two distinct cooling rates $\delta_{\text{SC}} = 2 \times 10^{-4}$ and $\delta_{\text{SC}} = 2 \times 10^{-9}$ down to $T_{\text{f}} = 0.05$, and a protocol mimicking the vapor deposition (VD) procedure using four different particle-deposition rates δ_{VD} with substrates at different temperatures T_{s}. The details concerning this protocol can be found in Ref. [34]; we selected for each deposition rate δ_{VD} the value of T_{s} that corresponds to the lowest inherent structure energy of the resulting glass, which gives $T_{\text{s}} = 0.18$ at $\delta_{\text{VD}} = 2 \times 10^{-3}$, $T_{\text{s}} = 0.16$ at $\delta_{\text{VD}} = 2 \times 10^{-5}$, $T_{\text{s}} = 0.14$ at $\delta_{\text{VD}} = 2 \times 10^{-6}$, and $T_{\text{s}} = 0.16$ at $\delta_{\text{VD}} = 2 \times 10^{-7}$.

Following each protocol, we prepare N_{s} independent glasses (to which we will refer here as *samples*), each corresponding to a distinct glass basin in the energy landscape. We have considered $N_{\text{s}} = 10$ for all the cases with the exception of the VD glasses obtained with the slowest particle deposition rate, where only five samples were considered. We define the inherent structure (IS) of a configuration as the energy minimum that is reached by minimizing the energy starting from that configuration [59]. The different protocols allow us to produce glasses with a wide range of inherent structure energies E_{IS} [Fig. 1(b) in the main text].

APPENDIX C: CLONING PROCEDURE

To study the vibrational anomalies of a glass basin, for each of these samples, we create N_{c} *clones*, which correspond to different configurations of the same glass state, using the following procedure:

(i) We first cool the initial configuration instantaneously to $T = T_{\text{clone}} = 0.05$, and let it relax until we observe no more aging in the height of the plateau (during 2^{14} time steps). This temperature is chosen because for $T < T_{\text{clone}}$, E_{IS} becomes independent of temperature for all the samples, and furthermore no diffusion is observed at T_{clone} (with the exception of the samples prepared by the fastest cooling and deposition rates, i.e., $\delta_{\text{SC}} = 2 \times 10^{-4}$ and $\delta_{\text{VD}} = 2 \times 10^{-3}$, respectively, where some diffusion is still observed at this temperature at long times). These two observations imply that at T_{clone} the configurations are trapped into well-defined glass basins, which is not always the case at the preparation temperature (T_{f} or T_{s} depending on the protocol), where residual diffusion and inherent structure energy variations are observed in some samples.

(ii) Stable glass configurations obtained at T_{clone} are then cloned by performing $N_{\text{c}} = 200$ short independent simulations assigning to each configuration a set of independent random velocities drawn from the Maxwell distribution at T_{clone}, as shown in the inset of Fig. 1 in the main text. The length of these simulations is chosen to be longer than the ballistic regime, to let the particles explore their inner cages (of average sizes Δ^{∞}). In our case, 2^{10} [the vertical dotted line in Fig. 2(a) in the main text] satisfied these requirements for all our samples.

The clones thus represent independent configurations of a same sample at the cloning temperature T_{clone}.

APPENDIX D: INSTANTANEOUS QUENCHES IN TEMPERATURE

Now, starting from each of these clones, we perform instantaneous quenches to lower temperatures. That is, we rescale the velocities of the particles in such a way that the kinetic energy corresponds to a temperature $T < T_{\text{clone}}$, and then we use standard molecular dynamics to follow the evolution of the system, keeping the temperature fixed by a Nosé-Hoover thermostat [56]. The initial time corresponds to the time of the quench, and we call t_{w} the time elapsed since the quench.

[1] M. L. Falk and J. S. Langer, Phys. Rev. E **57**, 7192 (1998).
[2] P. Schall, D. A. Weitz, and F. Spaepen, Science **318**, 1895 (2007).
[3] H. G. E. Hentschel, S. Karmakar, E. Lerner, and I. Procaccia, Phys. Rev. Lett. **104**, 025501 (2010).
[4] F. Puosi, J. Rottler, and J.-L. Barrat, Phys. Rev. E **94**, 032604 (2016).
[5] A. S. Keys, L. O. Hedges, J. P. Garrahan, S. C. Glotzer, and D. Chandler, Phys. Rev. X **1**, 021013 (2011).
[6] R. Candelier, A. Widmer-Cooper, J. K. Kummerfeld, O. Dauchot, G. Biroli, P. Harrowell, and D. R. Reichman, Phys. Rev. Lett. **105**, 135702 (2010).
[7] E. D. Cubuk, S. S. Schoenholz, J. M. Rieser, B. D. Malone, J. Rottler, D. J. Durian, E. Kaxiras, and A. J. Liu, Phys. Rev. Lett. **114**, 108001 (2015).
[8] V. K. Malinovsky and A. P. Sokolov, Solid State Commun. **57**, 757 (1986).
[9] R. Zeller and R. Pohl, Phys. Rev. B **4**, 2029 (1971).
[10] W. A. Phillips, Rep. Prog. Phys. **50**, 1657 (1987).
[11] D. L. Malandro and D. J. Lacks, J. Chem. Phys. **110**, 4593 (1999).
[12] J. Hachenberg, D. Bedorf, K. Samwer, R. Richert, A. Kahl, M. D. Demetriou, and W. L. Johnson, Appl. Phys. Lett. **92**, 131911 (2008).
[13] M. Goldstein, J. Chem. Phys. **132**, 041104 (2010).
[14] S. Capaccioli, M. Paluch, D. Prevosto, L.-M. Wang, and K. Ngai, J. Phys. Chem. Lett. **3**, 735 (2012).
[15] S. F. Swallen, K. L. Kearns, M. K. Mapes, Y. S. Kim, R. J. McMahon, M. D. Ediger, T. Wu, L. Yu, and S. Satija, Science **315**, 353 (2007).

[16] S. S. Dalal, A. Sepúlveda, G. K. Pribil, Z. Fakhraai, and M. Ediger, J. Chem. Phys. **136**, 204501 (2012).
[17] E. Leon-Gutierrez, A. Sepúlveda, G. Garcia, M. T. Clavaguera-Mora, and J. Rodríguez-Viejo, Phys. Chem. Chem. Phys. **12**, 14693 (2010).
[18] D. R. Queen, X. Liu, J. Karel, T. H. Metcalf, and F. Hellman, Phys. Rev. Lett. **110**, 135901 (2013).
[19] T. Pérez-Castañeda, C. Rodríguez-Tinoco, J. Rodríguez-Viejo, and M. A. Ramos, Proc. Natl. Acad. Sci. USA **111**, 11275 (2014).
[20] X. Liu, D. R. Queen, T. H. Metcalf, J. E. Karel, and F. Hellman, Phys. Rev. Lett. **113**, 025503 (2014).
[21] H. B. Yu, M. Tylinski, A. Guiseppi-Elie, M. D. Ediger, and R. Richert, Phys. Rev. Lett. **115**, 185501 (2015).
[22] M. Tylinski, Y. Chua, M. Beasley, C. Schick, and M. Ediger, J. Chem. Phys. **145**, 174506 (2016).
[23] M. Goldstein, J. Chem. Phys. **51**, 3728 (1969).
[24] F. H. Stillinger and T. A. Weber, Phys. Rev. A **28**, 2408 (1983).
[25] S. Sastry, P. G. Debenedetti, and F. H. Stillinger, Nature (London) **393**, 554 (1998).
[26] P. G. Debenedetti and F. H. Stillinger, Nature (London) **410**, 259 (2001).
[27] A. Heuer, J. Phys.: Condens. Matter **20**, 373101 (2008).
[28] P. Charbonneau, J. Kurchan, G. Parisi, P. Urbani, and F. Zamponi, Nat. Commun. **5**, 3725 (2014).
[29] J. Reinisch and A. Heuer, Phys. Rev. B **70**, 064201 (2004).
[30] T. F. Middleton and D. J. Wales, Phys. Rev. B **64**, 024205 (2001).
[31] P. Charbonneau, Y. Jin, G. Parisi, C. Rainone, B. Seoane, and F. Zamponi, Phys. Rev. E **92**, 012316 (2015).
[32] L. Berthier, P. Charbonneau, Y. Jin, G. Parisi, B. Seoane, and F. Zamponi, Proc. Natl. Acad. Sci. USA **113**, 8397 (2016).
[33] C. Scalliet, L. Berthier, and F. Zamponi, Phys. Rev. Lett. **119**, 205501 (2017).
[34] D. R. Reid, I. Lyubimov, M. Ediger, and J. J. De Pablo, Nat. Commun. **7**, 13062 (2016).
[35] J. Helfferich, I. Lyubimov, D. Reid, and J. J. de Pablo, Soft Matter **12**, 5898 (2016).
[36] A. Ninarello, L. Berthier, and D. Coslovich, Phys. Rev. X **7**, 021039 (2017).
[37] L. Berthier, P. Charbonneau, E. Flenner, and F. Zamponi, Phys. Rev. Lett. **119**, 188002 (2017).
[38] D. J. Amit and V. Martin-Mayor, *Field Theory, the Renormalization Group, and Critical Phenomena: Graphs to Computers* (World Scientific, Singapore, 2005).
[39] A. Seguin and O. Dauchot, Phys. Rev. Lett. **117**, 228001 (2016).
[40] A. Liu, S. Nagel, W. Van Saarloos, and M. Wyart, in *Dynamical Heterogeneities and Glasses*, edited by L. Berthier, G. Biroli, J.-P. Bouchaud, L. Cipelletti, and W. van Saarloos (Oxford University Press, Oxford, 2011).
[41] M. Müller and M. Wyart, Annu. Rev. Condens. Matter Phys. **6**, 177 (2015).
[42] C. Hicks, M. Wheatley, M. Godfrey, and M. Moore, arXiv:1708.05644.
[43] E. Lerner, G. Düring, and E. Bouchbinder, Phys. Rev. Lett. **117**, 035501 (2016).
[44] H. Mizuno, H. Shiba, and A. Ikeda, Proc. Natl. Acad. Sci. USA **114**, E9767 (2017).
[45] R. L. Jack and J. P. Garrahan, Phys. Rev. Lett. **116**, 055702 (2016).
[46] V. Lubchenko and P. G. Wolynes, Proc. Natl. Acad. Sci. USA **100**, 1515 (2003).
[47] E. Gardner, Nucl. Phys. B **257**, 747 (1985).
[48] P. Charbonneau, J. Kurchan, G. Parisi, P. Urbani, and F. Zamponi, Annu. Rev. Condens. Matter Phys. **8**, 265 (2017).
[49] P. Urbani and G. Biroli, Phys. Rev. B **91**, 100202 (2015).
[50] D. Larson, H. G. Katzgraber, M. A. Moore, and A. P. Young, Phys. Rev. B **87**, 024414 (2013).
[51] M. C. Angelini and G. Biroli, Phys. Rev. Lett. **114**, 095701 (2015).
[52] T. Aspelmeier, H. G. Katzgraber, D. Larson, M. A. Moore, M. Wittmann, and J. Yeo, Phys. Rev. E **93**, 032123 (2016).
[53] P. Charbonneau and S. Yaida, Phys. Rev. Lett. **118**, 215701 (2017).
[54] M. Baity-Jesi *et al.*, J. Stat. Mech. (2014) P05014.
[55] K. Geirhos, P. Lunkenheimer, and A. Loidl, arXiv:1711.00816.
[56] G. J. Martyna, M. L. Klein, and M. Tuckerman, J. Chem. Phys. **97**, 2635 (1992).
[57] E. Bitzek, P. Koskinen, F. Gähler, M. Moseler, and P. Gumbsch, Phys. Rev. Lett. **97**, 170201 (2006).
[58] S. Plimpton, J. Comput. Phys. **117**, 1 (1995).
[59] F. H. Stillinger and T. A. Weber, Phys. Rev. A **25**, 978 (1982).